frontiers in Physics

REVIEW
published: 01 March 2022
doi: 10.3389/fphy.2022.727718

Target Characteristics Used in Laser-Plasma Acceleration of Protons Based on the TNSA Mechanism

*A. Măgureanu[1,2], L. Dincă[1,2], C. Jalbă[1,2], R. F. Andrei[3], I. Burducea[3], D. G. Ghiță[1], V. Nastasa[1], M. Gugiu[1], T. Asavei[1], O. Budrigă[4], D. Ticoş[4], V. Crăciun[1,4], B. Diaconescu[1] and C. M. Ticoş[1,2]**

[1]Extreme Light Infrastructure-Nuclear Physics (ELI-NP), Horia Hulubei National Institute for Physics and Nuclear Engineering (IFIN-HH), Măgurele, Romania, [2]Engineering and Applications of Lasers and Accelerators Doctoral School (SDIALA), University Politehnica of Bucharest, Bucharest, Romania, [3]Horia Hulubei National Institute for Physics and Nuclear Engineering (IFIN-HH), Măgurele, Romania, [4]National Institute for Laser, Plasma and Radiation Physics (INFLPR), Măgurele, Romania

The target normal sheath acceleration is a robust mechanism for proton and ion acceleration from solid targets when irradiated by a high power laser. Since its discovery extensive studies have been carried out to enhance the acceleration process either by optimizing the laser pulse delivered onto the target or by utilizing targets with particular features. Targets with different morphologies such as the geometrical shape (thin foil, cone, spherical, foam-like, etc.), with different structures (multi-layer, nano- or micro-structured with periodic striations, rods, pillars, holes, etc.) and made of different materials (metals, plastics, etc.) have been proposed and utilized. Here we review some recent experiments and characterize from the target point of view the generation of protons with the highest energy.

Keywords: laser, target, TNSA, proton acceleration, nano and micro

OPEN ACCESS

Edited by:
Antonino Picciotto,
Bruno Kessler Foundation (FBK), Italy

Reviewed by:
Dimitri Batani,
Université de Bordeaux, France
Zsolt Lécz,
ELI-ALPS Research Institute, Hungary

****Correspondence:***
C. M. Ticoş
catalin.ticos@eli-np.ro

Specialty section:
This article was submitted to Interdisciplinary Physics, a section of the journal Frontiers in Physics

Received: *19 June 2021*
Accepted: *07 February 2022*
Published: *01 March 2022*

Citation:
Măgureanu A, Dincă L, Jalbă C, Andrei RF, Burducea I, Ghiță DG, Nastasa V, Gugiu M, Asavei T, Budrigă O, Ticoş D, Crăciun V, Diaconescu B and Ticoş CM (2022) Target Characteristics Used in Laser-Plasma Acceleration of Protons Based on the TNSA Mechanism. Front. Phys. 10:727718. doi: 10.3389/fphy.2022.727718

1 INTRODUCTION

The record high electric fields (~ 10^6 V μm^{-1}) produced by ultra-high power lasers is a key feature that is being exploited for acceleration of sub-atomic particles [1]. In an unprecedented effort in the last 2 decades or so, many groups have been striving to push the limit of proton acceleration beyond the 100 MeV threshold. The highest energy attained so far is at about 94–98 MeV [2, 3]. Breaking this barrier opens up a full range of potential applications, just to mention a few, from nuclear fusion to radiography, or to medical use in tumour therapy. In the latest case one essential requirement is the proton kinetic energy in the few hundred MeV range (at an optimum of 250 MeV for deep tissue penetration), along with several other beam parameters that need an improvement such as an optimized energy spectrum range that can be adequately fitted to the required tissue penetration and a much lower divergence than it is currently obtainable. The majority of early experiments have been carried out with flat foil targets. The acceleration mechanism at work was identified as the target normal sheath acceleration (TNSA) in which the electrons accelerated by the laser pulse pass trough the target and create a spatial charge very close to its rear side [4]. The temperature of the escaping electrons resulted from the produced plasma was found to be a key parameter in the process.

Scans in both laser parameter space and target thickness have been carried out in order to identify the optimum acceleration regime [5, 6]. One of the main laser parameter is the pulse duration which has been decreased over the years from picosecond level to 20–30 fs. This has been possible due to the chirped pulse amplification (CPA) technique invented by D. Strickland and G. Mourou [7]. It

appeared first that a threshold in proton energy at around 60 MeV was difficult to overcome [6]. A breakthrough has been possible when the geometry of the target was changed: a flat-top cone target with the large opening aimed towards the laser pulse proved to produce higher energy protons than an equivalent flat target, at the same laser parameters [8]. These early findings clearly demonstrated the role of the hot electrons, in this particular case of the electrons trapped from the cone surface and heated up to higher temperature by direct laser acceleration.

It was shown that the "p" polarization state of the laser pulse is more favorable to electron heating than the "s" polarization, as a resonant absorption takes place with the outermost surface electrons embedded in the prepulse plasma oscillating early in the incident laser field [9]. Reflection of the laser pulse by the plasma found at the critical density and the implicit loss of incident power is another key factor in this equation [10]. In the quest to provide a unitary solution to all these aspects, i.e., more intense heating of electrons, inward reflection of the laser light and higher density surface electrons, different morphologies have been considered: nanospheres, nanorods, micropillars, foams or gratings embedded in the target surface. In the following we attempt to capture how the morphology of the solid target and its composition is transposed into higher proton energy, taking into consideration also the laser parameters.

To know the end result of using a particular type of target is of paramount importance for ELI-NP as its experimental areas become gradually operational and soon proton and ion acceleration experiments will be carried out [11, 12]. There are two experimental areas dedicated to irradiation of solid targets with laser pulses peaked at 1 PW (in E5 area) and 10 PW (in E1 area), equipped with focusing mirrors with short focal length having *f*/3.5 and *f*/2.7, respectively, with a full beam diameter of ~ 20 and ~ 55 cm, respectively. Also a target laboratory is available at ELI-NP where targets can be designed and fabricated in-house [13].

In this paper we review from the literature the results of using different target morphologies in terms of maximum obtained proton energy without examining the peculiarities of the TNSA mechanism, nor the related energy scaling laws [6, 14–17]. We focus on foil targets with thickness in the micron range, on micrometer size spherical targets, on micro- and nanostructured targets with surface features at/or below the 1 μm level, and on conical targets with characteristics (such as the large cone opening) which extend well beyond 100 μm. Most of these targets are made of metals (Al, Ag, Au, Cu, Fe, Mo, Pd, stainless steel, Sn, Ti), plastic (dielectric) and other non-metallic materials. Our review is rather intended as a guide among the multitude of reported results and can possibly become the premise of a subsequent more elaborate study. We do however mention the main features of the utilized experimental setups and findings. This approach will help us identify some trends in target fabrication and give us a rough estimate on what to expect upon irradiation with ultra-short laser pulses.

2 TNSA MECHANISM OF PROTON ACCELERATION

We review very briefly a few basic characteristics of the TNSA mechanism for proton and ion acceleration by high power laser pulses on flat targets. The focused laser in a spot of the order of a few microns with intensity above 10^{18} W cm^{-2} ionizes the target and accelerates the electrons to relativistic energies (in the 100's keV to MeV range) via the ponderomotive force. These "hot" electrons cross the target, exit from the opposite side and create a spatial charge near the back surface. A sheath forms at the back of the target with a spatial scale of 1–10 μm within a time period in the ps range. The intense electric field created inside this sheath is $E_s = \sqrt{2}k_BT_{hot}/e\lambda_D$, where T_{hot} is the temperature of the hot electrons, $\lambda_D = \sqrt{\epsilon_0 k_B T_{hot}/e^2 n_e}$ is the Debye length (or the plasma screening length) and n_e is the electron density [4]. For $k_BT_{hot} = 1$ MeV, $n_e = 3 \times 10^{19}$ cm^{-3}, $\lambda_D = 10^{-6}$m and we obtain $E_s \sim 10^{12}$ Vm^{-1}. If electrons with energy 1 MeV flow through a simple Al foil (with no laser irradiation), their combined radiative and collisional stopping power is of order 0.4 keV μm^{-1} [18]. This situation changes as the target becomes a fully ionized plasma during laser irradiaton and the dynamics of electron acceleration is affected by the creation of the opposed sheath electric field at the back of the target which leads to the generation of return currents [19]. It has been shown that the stopping power of an Al plasma can be several times higher than that of a simple Al foil, for hot electrons [20–22].

The atoms on the back side of the target become fully ionized by this high field E_s and the protons coming from surface contaminants (such as H_2O or hydrocarbons compounds found in the oil of vacuum equipments) and target ions are swiftly accelerated within this sheath region. One can see straightforwardly that the field increases if electrons are hotter, the plasma becomes denser and the Debye length is reduced. The electron temperature consistent with the scaling of the ponderomotive force is proportional with the laser intensity I and wavelength λ_L [23, 24]: $k_BT_{hot} = 1\,\text{MeV} \times \sqrt{I{\lambda_L}^2/10^{19}\ \text{Wcm}^{-2}\ \mu\text{m}^{-2}}$. Thus for a laser with $\lambda_L = 800$ nm and $I = 2 \times 10^{19}$ W cm^{-2} one obtain an electron temperature $k_BT_{hot} = 1.13$ MeV.

Another aspect which is less stringent for thick targets (of order of tens of micrometers) but extremely important for very thin ($\lesssim 1\ \mu$m) or nanostructured targets is the irradiation by the prepulse due to amplified spontaneous emission. The intensity achieved during prepulse irradiation has to be well below the ionization threshold ($\approx 10^{11} - 10^{13}$ W cm^{-2}) in order to not affect the integrity of the target or ionize it before the arrival of the main laser pulse [25, 26]. A common technique for lowering the prepulse and increase the contrast (i.e., the ratio between the pulse and its prepulse at given moments in time, from ns to few ps) is the reflection of the main laser pulse off a single or double plasma mirror, which could come at the expense of lowering its peak intensity (e.g., up to 20%) [27, 28]. Still, the prepulse can be used to good advantage to enhance ion acceleration if it is produced in a controllable manner, with defined duration and intensity [15].

3 TARGET CHARACTERISTICS

3.1 Metallic Targets

Aluminum is one of the most common materials used for target fabrication. Some of the first reported results were obtained with Al

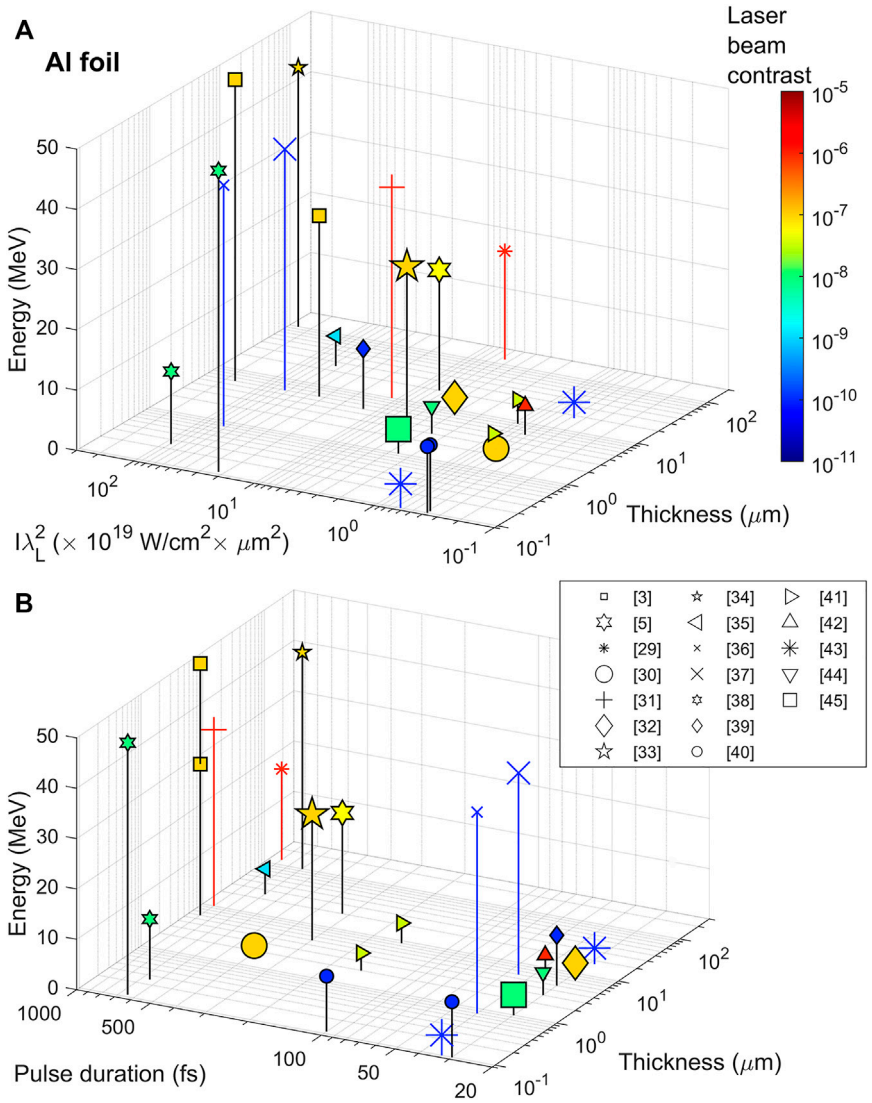

FIGURE 1 | Maximum energy of protons accelerated from targets made of Al foil with the corresponding reference (as given in the legend for all data points): 50 MeV [3, 38], 43 MeV [34], 40 MeV [36, 37], 35 MeV [31], 30 MeV [3], 28 MeV [37], 20 MeV [5], 18 MeV [29],12.6 MeV [38], 11 MeV [40], 10 MeV [39], 5 MeV [35], 4.8 MeV [42], 4.5 MeV [44], 4 MeV [41, 43, 45], 3.5 MeV [41], 2 MeV [32], 1.5 MeV [30], 0.6 MeV [43] in **(A)** vs the product of laser intensity and squared laser wavelength $I\lambda_L^2$ and target thickness, and **(B)** vs laser pulse duration and target thickness. The color of the data points is according to the contrast of the laser beam shown in the color bar. The contrast values are given in the above references, typically for a few picoseconds or tens of picoseconds before the main pulse.

thin films [29–32]. The reported maximum energy of protons is shown in **Figure 1**, depending on the target thickness and laser intensity in (A) and on pulse duration in (B). The typical target thickness varies from bellow 1 μm to few 10's μm and even several 100's μm. In **Figure 1A** one can distinguish between two groups, depending on the peak energy value. The first group is characterized by a high laser intensity $I\lambda_L^2 \gtrsim 4 \times 10^{19}$ W cm^{-2} μm^2 [3, 5, 29, 31, 33–40]. In this group the peaks have consistently higher energy, between 18 and 50 MeV, with a few exceptions at 5, 10, 11 and 12.6 MeV [35, 38–40]. The second group is positioned below the value $I\lambda_L^2 \lesssim 2 \times 10^{19}$ W cm^{-2} μm^2 [30, 32, 41–45]. Interestingly, all maximum proton energies of the second group are lower by an order of magnitude, between 0.6 and 4.8 MeV.

Based on pulse duration we can see in **Figure 1B** three groups of results: for pulses $\lesssim$45 fs, between 100 and 320 fs, and those near the 1 ps level, at 0.7–0.9 ps. It appears that a higher laser intensity associated with longer pulses (in the few 100's fs) led to higher proton maximum energies, above 20 MeV. However, there are two high peak values obtained for short pulses (i.e., at 40–45 fs) which stand out: 28 MeV, for a 2 μm thick foil [37] and 40 MeV for a 0.6 μm thick foil [36]. In these two cases the contrast was 10^{-10}. Concerning the dependence of proton energy on the pulse duration, Zeil et al. showed a linear scaling of maximum proton energy with the laser intensity for short pulses, in the tens of fs, and a square root scaling with laser intensity for longer pulses, with duration in the several hundred fs

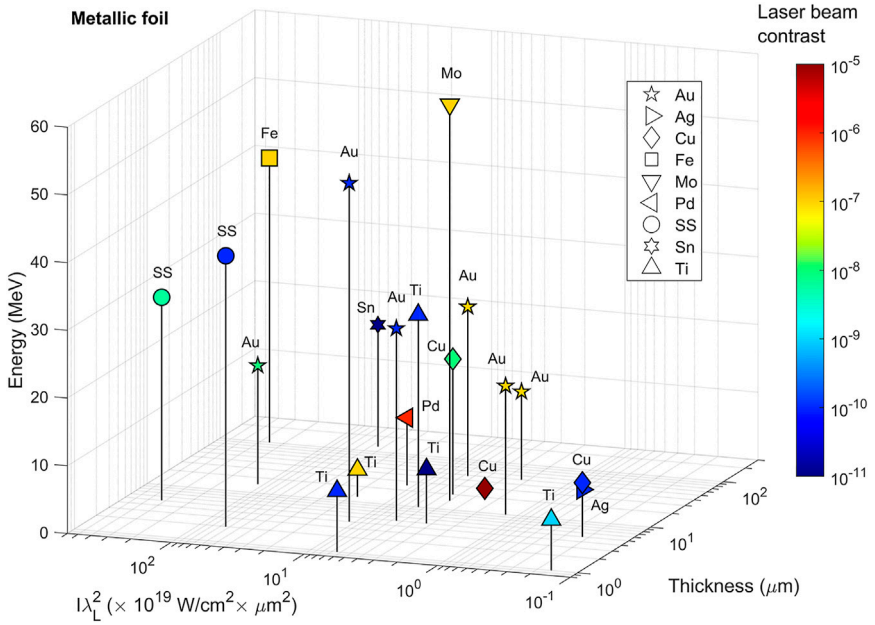

FIGURE 2 | Maximum energy of protons accelerated from targets made of different metals as follows: Au (50 MeV [50], 28.4 MeV [49], 25 MeV [46], 19 MeV [8], 17.5 MeV [48], 13 MeV [47]), Ag (7 MeV [51]), Cu (20 MeV [53], 8 MeV [51], 1.3 MeV [52]), Fe (42 MeV [54]), Mo (58.5 MeV [6]), Pd (10 MeV [35]), stainless steel-SS (40 MeV [36], 30 MeV [55]), Sn (18 MeV [56]) and Ti (28.4 MeV [49], 9 MeV [28], 8 MeV [57], 7.5 MeV [58], 4 MeV [59]) vs the product of laser intensity and squared laser wavelength $I\lambda_L^2$ and target thickness. The data points are colored according to the contrast of the laser beam shown in the color bar. The contrast values are given in the above references, typically for a few picoseconds or tens of picoseconds before the main pulse.

duration and up to 1 ps [15]. From the contrast point of view the highest cut-off energies are obtained with a contrast better than 10^{-7}, regardless of the target thickness.

Targets made of other types of metals have been tested as well, as shown in **Figure 2**. Results obtained at different facilities by employing foils of Au [8, 46–50], Ag [51], Cu [51–53], Fe [54], Mo [6], Pd [35], stainless steel (SS) [36, 55], Sn [56], Ti [28, 49, 57–59] are plotted against $I\lambda_L^2$ and the foil thickness. A central group of relatively high energy values for different types of metallic targets (Mo, Au, Cu, Ti, Sn) appears in a parameter space characterized by an intensity $10^{19} < I\lambda_L^2 < 2 \times 10^{20}$ W cm^{-2} μm^2 and target thickness between 4 and 50 μm. It seems that no energy increase is evident with a particular type of metal. The peak energy is obtained with Mo, Au, Fe and SS targets. With a measured top proton energy near 60 MeV, the flat metallic targets considered in **Figures 1** and **2** do not lead to the record proton energies, as it is shown in the followings, where other types of target material are considered. Nevertheless they constitute a very useful tool for benchmarking the main laser pulse features and the diagnostics for proton and ion beam characterization. As in the case of Al targets the highest cut-off energies are obtained with a laser beam contrast better than 10^{-7}.

3.2 Dielectric and Non-Metallic Targets

In order to maximize the protons flux obtained from a target and not rely solely on its inherent surface contaminants rich in H atoms, including here water vapours or other compounds (e.g., alcohol), a straightforward solution was to fabricate the targets out of materials containing a high density of C-H bonds. Typical materials are those made of plastic. Examples are foils made of parylene-N $(C_{16}H_{16})_n$, polyethylene $(C_2H_4)_n$, polystyrene or PS $(C_8H_8)_n$ often abbreviated as CH, Mylar or PET $(C_{10}H_8O_4)$, Kapton $(C_{22}H_{10}O_5N_2)_n$, polymethyl methacrylate or PMMA $(C_5O_2H_8)_n$, polymethylpentene or PMP $(C_6H_{12})_n$, also known as TPX, etc, or liquid targets that can be well manipulated in terms of thickness and surface and are compatible with high vacuum. Other tested non-metallic materials were C, Si and SiN.

One of the first results which stood several years as a record for proton energy at 58 MeV was obtained using a 100 μm foil made of PS [1]. In **Figure 3** we present results obtained with targets made of different plastic foils: PS [1–3, 24, 60, 61], Mylar [32, 62–67], PMP [50], Kapton [68], SiN [65, 69], amorphous Carbon [70], synthetic diamond (CVD) [38], liquid crystals-8CB [71], and a pure Si substrate [72].

In **Figure 3A** we can distinguish two groups well separated by the value of $I\lambda^2$: below 4×10^{19} W cm^{-2} μm^2 and above 10^{20} W cm^{-2} μm^2. In the first group the target thickness varies over a wide range, from ~ 0.1 to ~ 400 μm, while the proton maximum energy is relatively low, between 2 and 10 MeV. The second group features much higher proton energy, up to 98 MeV. The thicknesses that lead to the highest proton energy ($\geq$60 MeV) appear to be between ~ 100 nm–1.5 μm [2, 40, 50, 61]. These results have been obtained at intensities in the range 10^{20}–1.5×10^{21} W cm^{-2} μm^2. Bellow the 1 μm threshold for target

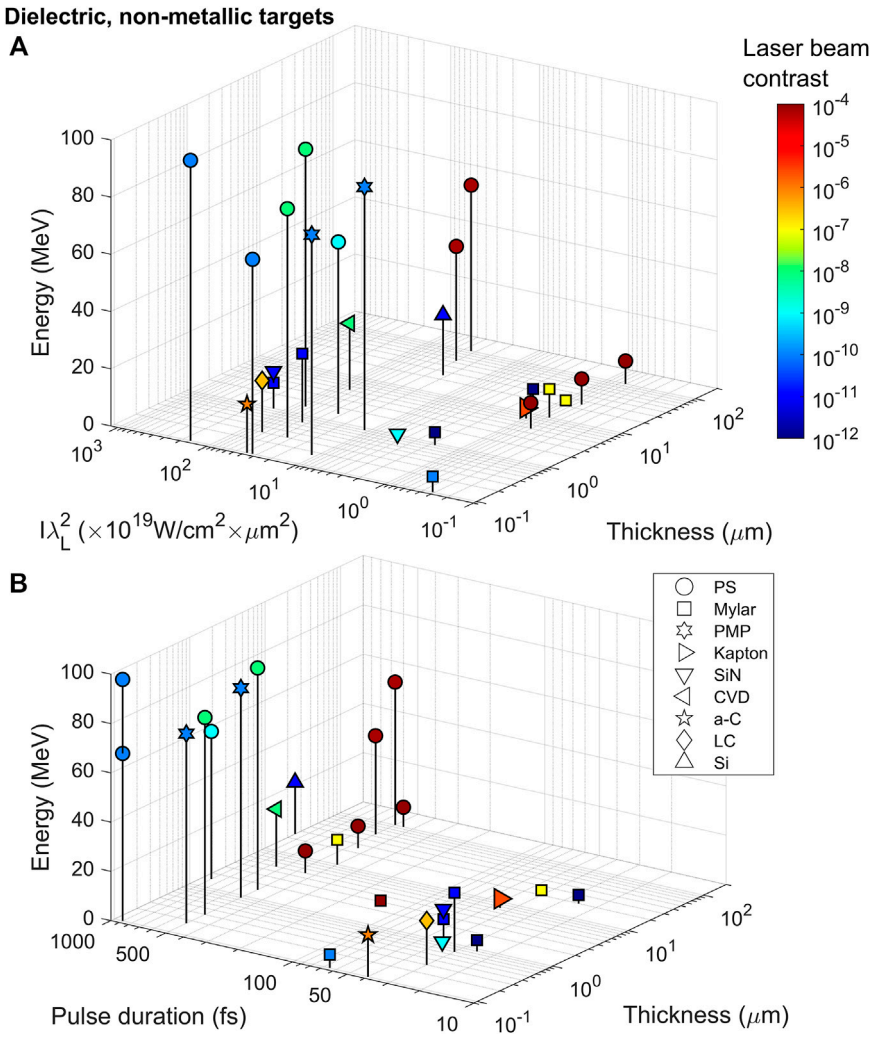

FIGURE 3 | Maximum energy of protons accelerated from targets made of plastic or insulating sheet: **(A)** vs the product of laser intensity and squared laser wavelength $I\lambda_L^2$ and target thickness, and **(B)** vs laser pulse duration and target thickness. Different types of plastic materials are considered: PS (68 and 98 MeV [3], 80 and 90 MeV [61], 60 MeV [2], 58 MeV [1], 40 MeV [24], 8 and 9 MeV [60]), Mylar (24 MeV [67], 10 MeV [32], 9 MeV [65], 5.5 MeV [64], 3.5 and 4.5 MeV [66], 2.2 MeV [62], 2 MeV [63]), PMP (77 and 85 MeV [50]), Kapton (3.8 MeV [68]), as well as some types of insulating or semiconductor materials such as SiN (13 MeV [65], 3 MeV [69]) synthetic diamonds (CVD) (23.3 MeV [38]), amorphous Carbon (a-C) (17 MeV [70]), liquid crystal (LC) (18 MeV [71]) and pure Si (21 MeV [72]). The data points are colored according to the contrast of the laser beam shown in the color bar. The contrast values are given in the above references, typically for a few picoseconds or tens of picoseconds before the main pulse.

thickness the onset of the relativistic induced transparency (RIT) regime [2] and radiation pressure acceleration (RPA) mechanism [10] have to be accounted for, in combination with the TNSA mechanism.

The higher proton energy reported for plastic targets, with several peaks surpassing 60 MeV [3, 50, 61] can be due to the increased coupling of the laser light into the target as demonstrated by Geng et al. [73]. When plotted against the pulse duration, the results are again well separated, most high peaks being obtained for pulses longer than 400 fs, as shown in **Figure 3B**. For ultrashort laser pulses, in the tens of femtoseconds, the record proton energy is 24 MeV for a target made of Mylar with a thickness of 0.7 μm [67]. The contrast of the peak cut-off energies is better than 10^{-8}, although relatively high proton energies are obtained with thick targets and low contrast, of order 10^{-4} – 10^{-5}.

3.3 Conical Targets

The first results were reported on the TRIDENT laser at Los Alamos by K. A. Flippo et al. using a flat-top conical target [8]. They showed a proton cutoff energy of 30 MeV, compared to 19 MeV for its counterpart, a thin gold foil with 10 μm thickness. The laser intensity was 1.1×10^{19} W cm^{-2}, the energy in the beam was 18.7 J, the pulse duration was ~ 600 fs, and the contrast was 10^{-7} at the central wavelength 1.054 μm. The conical target was also made of Au with a flat top diameter 100 μm and wall thickness 10 μm, having a neck at the apex of 20 μm, a large opening of ~ 400 μm and a length 200 μm.

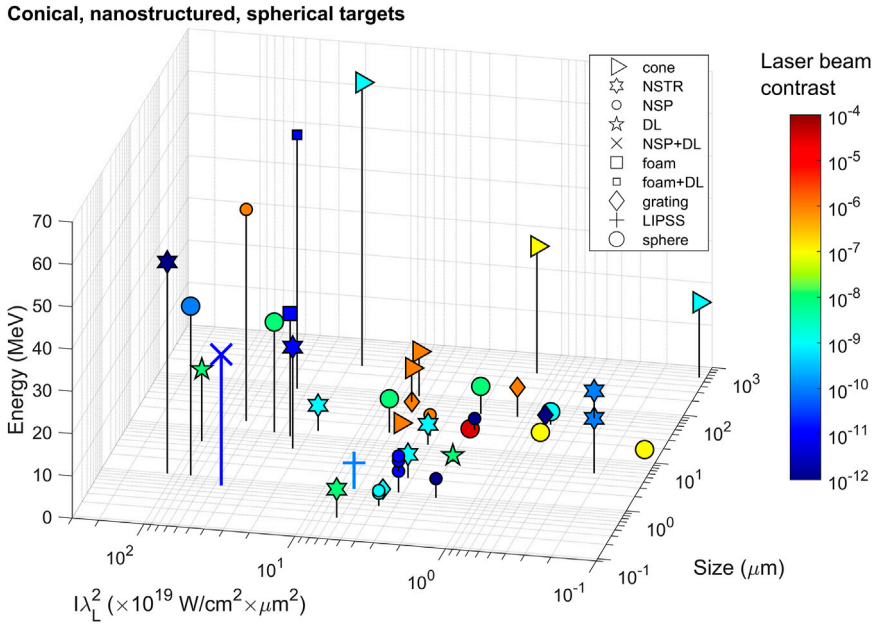

FIGURE 4 | Maximum energy of protons accelerated from targets with different morphology vs the product of laser intensity and squared laser wavelength $I\lambda_L^2$ and target thickness. "cone" refers to flat-top cones (67 MeV [74], 30 MeV [8], 17.8 MeV [76], 1, 9.5 and 10.5 MeV [75]), "NSTR" means nano- and microstructured targets having nanowires (4.8 and 5.6 MeV [88]), micropillars (24 MeV [72], 13 and 19.5 MeV [51]), microtubes (50 MeV [89]), nanochannels (6 MeV [59]), nanoholes (6.7 MeV [90]), "NSP" refers to nanospheres (5, 7.5 and 8.6 MeV [92], 3.5 and 4.5 MeV [66], 3 and 3.6 MeV [69]) and nanoparticles (3.7, 5 and 50 MeV [91]) embedded onto the surface, "DL" describes a target made of a double layer (1.5 MeV [93], 17 MeV [38]), "NSP + DL" describes a combination of double-layer and nanospheres embedded onto the surface (31 MeV [67]), "foam" refers to target consisting of a foam on top of a flat layer (29 MeV [95]), foam + DL refers to foam on a double layer (60 MeV [96]), "grating" describes the grating-like surface of the target (1.5 and 7 MeV [97], 5 MeV [98], 2.3 MeV [69]), "LIPSS" refers to a target which features periodic structures on the surface obtained by laser engineering (6.1 MeV [28]), and "sphere" refers to droplets or spherical targets (40 MeV [82], 25 MeV [87], 8 MeV [86], 6.5 MeV [85], 3 MeV [84], 1.5 MeV [83], 1 MeV [81], 0.6 MeV [80]. The "size" refers to the overall thickness of the substrate. The data points are colored according to the contrast of the laser beam shown in the color bar. The contrast values are given in the above references, typically for a few picoseconds or tens of picoseconds before the main pulse.

Later on, in another series of experiments at the same laser facility, this time by utilizing cone targets made of Cu, the proton cut-off energy was higher, at 67 ± 2 MeV [74]. The laser intensity was an order of magnitude higher 1.5 (±0.5) × 10^{20} W cm^{-2}, while the laser had an energy 82 ± 15 J and a pulse duration 670 ± 130 fs. The contrast was 10^{-9} at 80 ps before the main pulse. The target had the flat top diameter of 290 μm and wall thickness 12.5 ± 2.5 μm, a neck of 160 μm, an opening about the same size as the top, and a height of 100 μm.

The results of cone target experiments are presented in **Figure 4** [8, 74–76], referenced to the large opening of the cone which is in the 10s or 100*s* of μm. Flat-top cones with smaller openings, ranging from 20 to 90 μm produced protons with maximum energies in the 1–10.5 MeV range, with the top hat foil diameter betwen 30 to 300 μm [75]. Foord et al. obtained 17.8 MeV by using as target a spherical shell with thickness 10 μm and radius 300 μm attached to a large empty cone made of Al [76]. In all presented cases above the wall of the cone had a relatively similar thickness, 10 to 12.5 μm.

The main benefits of cone targets appear to be an increased confinement of the laser light inside the cone and a more effective generation of hot electrons from the inner cone walls. In fact, numerical simulations have shown that inside a conical target the internal reflections of the laser beam towards the cone apex leads to a smaller focusing spot which increases the laser intensity with orders of magnitude, and also the electron density increases due to surface electron induced-flow [77, 78].

3.4 Spherical Targets

The idea of using a target with a limited size also known as "mass-limited" which can lead to an improved confinement of the deposited laser energy was first tested by Buffechoux et al. [79] who showed the generation of a more uniform plasma sheath connecting both sides of a thin foil target (facing and opposed to laser irradiation). They demonstrated a threefold increase in proton energy at an intensity of 2 × 10^{19} W cm^{-2}, explained by the propagation of a transverse reflux of electrons crossing the edge of the target. A particular category of "mass-limited" targets is that of microspheres with specific structural properties, including here droplets. Levitated spheres or spherical shells with sizes in the micron range have been exposed to high power laser pulses, as shown in **Figure 4**.

A first challenge is to levitate the sphere in high vacuum in a very stable equilibrium position, with temporal drifts less then a few microns. There are several known techniques such as optical levitation or quadrupole trapping. In the first case the radiation pressure provided by an auxiliary laser beam is pointing upward, compensating for the target weight and trapping is realized in the

focal spot by the ponderomotive force. In the second case the configuration of the electric field between 4 quadrupoles is such that the target is levitated at mid distance from the poles, along the axis of the trap [80, 81]. It should be emphasised that one advantage of such a target configuration is its physical detachment from any support. Thus, during the laser shot the electron flow between the target and the chambers walls wich arises to equilibrate the expelled charges during the acceleration phase is prevented. This can possibly lower the generation of giant electromagnetic noise pulses.

Polystyrene spheres and hollow spheres covered with PMMA, having a 1 μm diameter, produced proton cut-off energies up to ≈ 40 MeV at the PHELIX laser facility [82]. The pulse had an intensity 7×10^{20} Wcm^{-2} in a spot with $\sim 3.7 \pm 0.3$ μm in diameter by focusing a fraction of the full energy 150 J delivered within 500 fs. A particular feature was the very narrow energy spread of the proton bunch at FWHM, of order of 10% or less, probably due to a much more localized plasma, in a volume with a radius ~ 7 μm. Here the results have been explained by including in the model the Coulomb repulsion between the protons and the microparticle ions. A much lower proton energy, in the range 0.6–1 MeV, has been demonstrated by Sokolik et al. [80, 81] by using water and glass droplets with a larger size ($\gtrsim$ 11 μm) and a laser intensity 10^{18}–10^{19} W cm^{-2} with a pulse duration of 45–60 fs and temporal contrast 10^{-7} – 10^{-8}. Water droplets have also been used in experiments by Schnürer et al. [83] and Becker et al. [84]. In [83] protons were accelerated up to 1.5 MeV at a laser intensity 10^{19} W cm^{-2} from 20 μm droplets, while in [84] 3 MeV protons were obtained with a frequency doubled pulsed laser at λ = 400 nm and intensity 4×10^{19} W cm^{-2} from free falling water droplets with a mean diameter of 40 μm. Glass micropsheres coated with a 50 nm silver layer having 50 μm in diameter generated 6.5 MeV protons at 3 $\times 10^{19}$ W cm^{-2} [85]. Microspheres made of plastic (PMMA and PS) have produced protons with 8 and 25 MeV, respectively. In the first case their size was 15 μm and irradiated by a pulse with 10^{20} W cm^{-2} [86], while in the second case the spheres had 10 μm in diameter matching the laser focal spot and were exposed to an intensity of 2 – 3 $\times 10^{20}$ W cm^{-2} [87].

3.5 Nano- and Micro-Structured Targets

A paradigm shift has been seen in the last years in the target morphology, from simple flat foils to micro- and nano-structured targets presented in several reports, in order to highlight the benefit of the latests. Targets consisting of nanowires [88], micropillars and microtubes [51, 72, 89], nanochannels [59], nanoholes [90], flat foils embedded with nanoparticles [91] or with nanospheres [66, 69, 92], double layers made of different materials [38, 93], a combination of double-layer and embedded nanospheres [67], foams [94–96] and flat foil with grooves or micro-gratings [28, 69, 97, 98] have already been tested. The results reported with these types of targets are presented also in **Figure 4**. This transition has been determined by the need of optimized laser absorption in the created plasma, more controlled heating of the electrons in order to reach higher accelerating fields, and the availability of equipments and techniques that can deliver such interconnected small parts. One prerequisite for the use of such targets is a good contrast of the laser pulse, otherwise the prepulse can ionize and wash away the spatial features of the target surface when the main pulse arrives. The optimum range is at least beyond 10^{-9} [59] and goes up to 10^{-11}..10^{-12} [72] by utilizing two plasma mirrors.

There are several interesting comparisons between flat foils and micro- or nano-structured targets. Some recent results with flat foils (made of metals or plastic) have been included in the previous subchapters, and in **Figures 1**, **2**, and **3**. In several studies it is demonstrated that the maximum proton energy increases with the use of these types of targets. Vallierres et al. (2019) obtained 50 MeV for a surface embedded with Ag and Au nanospheres on an Al foil compared to 40 MeV for the bare surface, at an intensity of 5×10^{20} W cm^{-2}, and 5 and 3.7 MeV against 3.1 MeV for the same comparison (with Au and Ag nanospheres, respectively) but at a lower intensity 3×10^{19} W cm^{-2} [91]. A maximum proton energy of 5.6 MeV has been obtained for a target featuring nanowires on a Cu surface compared to 3.2 MeV for a flat target in [88], and 6.1 MeV for a periodic striated Ti target compared to 5 MeV for the simple Ti foil in [28]. Ebert et al. showed an increase ≈ 24 vs 21 MeV by employing a surface structure covered with Si cones, each with a base width of 5 μm and height 15 μm, having a "forest-like" aspect [72].

On the other hand there have been also a few reports which did not show an enhancement of the maximum proton energy in spite of the use of nanostructured targets. In [69] it is shown that the use of a SiN membrane with grating structure decreases the proton energy to 2.3 MeV from the reference 3 MeV obtained with a bare foil, at a laser intensity of 6×10^{19} W cm^{-2}. Floquet et al. did not see any improvement above 4.5 MeV obtained by employing a mylar foil (0.9 and 20 μm in thickness) embedded with PS nanospheres having 471 and 940 nm in diameter at a laser intensity 2.8×10^{19} W cm^{-2} [66].

In [72] it is shown also that the flux of protons increases by a factor of 4.4 by using the micro-structured target, exposed to laser pulses with energy 160 ± 30 J, pulse duration 1 ± 0.1 ps, contrast 10^{-11} achieved by employing a double-plasma mirror, and peak intensity $2 \pm 0.1 \times 10^{20}$ W cm^{-2} in a 10 μm round focused spot. The reference result was provided by a flat Si foil with 25 μm thickness. A tremendous increase by an order of magnitude was seen in the later case in the intensity of emitted X-rays, i.e. of the full spectrum and of the K_α line.

As opposed to the bare thin foils, the nanostructred targets due to their low density structure can lead to the formation of a controlled near-critical plasma layer on the illuminated side, allowing the laser pulse to penetrate deeper into the target. This can favor an enhanced laser energy absorption within a larger plasma volume and a more efficient heating of the electrons, improving the conditions for ion acceleration. In fact, in the experiments with foam targets the plasma formed at the top of the foam covering either a foil or a double layer stayed slightly under-dense [95, 96]. These conditions can be used for accessing the collisionless shock acceleration regime as a potential mechanism for achieving higher cut-off energies.

3.6 Narrow Pulse Duration Range and Different Targets

A comparison of all previously discussed types of targets is shown in **Figure 5**, but for only a narrow pulse duration range (≈ 25 to

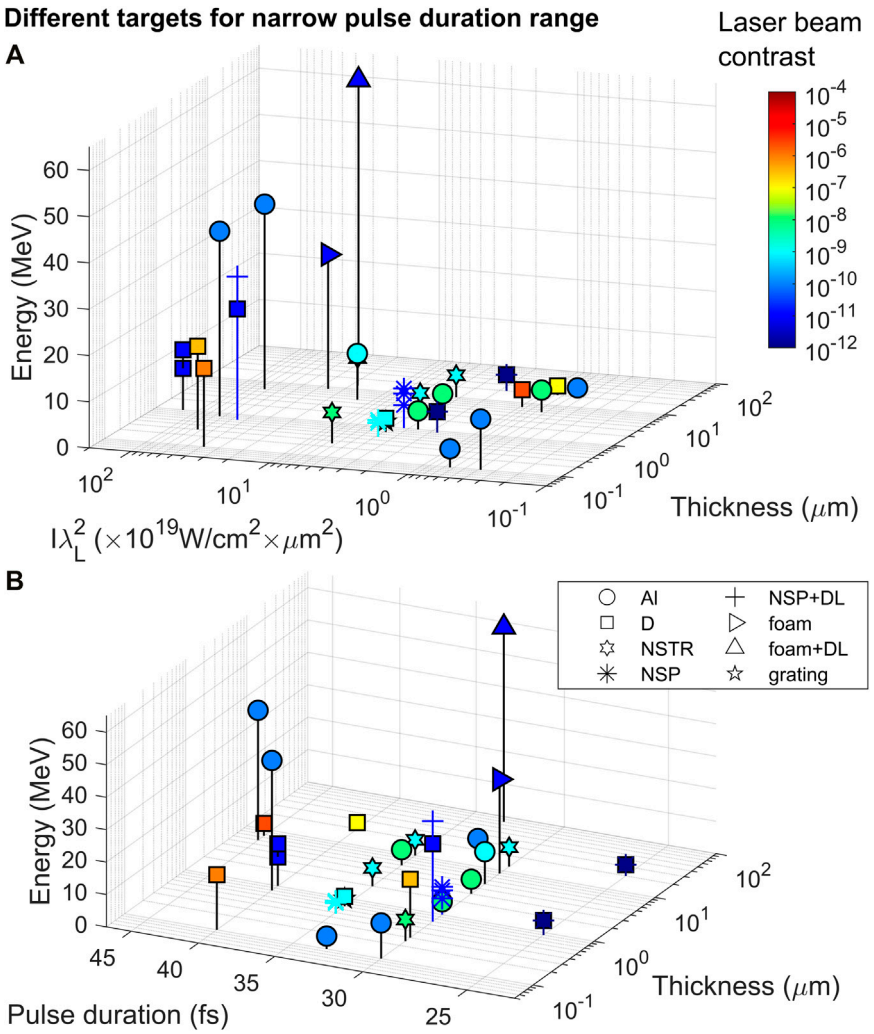

FIGURE 5 | Maximum energy of protons accelerated from different types of targets: **(A)** vs the product of laser intensity and squared laser wavelength $I\lambda_L^2$ and target thickness, and **(B)** vs laser pulse duration and target thickness. The targets are Al foils "Al" (40 MeV [36, 37], 11 MeV [40], 10 MeV [39], 4.8 MeV [42], 4.5 MeV [44], 4 MeV [43, 45], 0.6 MeV [43], dielectric and non-metallic foils "D", i.e., Mylar (24 MeV [67], 9 MeV [65], 3.5 and 4.5 MeV [66], 2 MeV [63]), Kapton (3.8 MeV [68]), SiN (13 MeV [65], 3 MeV [69]), liquid crystal (18 MeV [71]) and amorphous carbon (17 MeV [70]), nano-and microstructured foils "NSTR" i.e., nanowires (4.8 and 5.6 MeV [88]), nanoholes (6.7 MeV [90]), nanochannels (6 MeV [59]), nanospheres "NSP" (5, 7.5 and 8.6 MeV [92], 3.5 and 4.5 MeV [66], 3 and 3.6 MeV [69]), nanospheres on a double layer target "NSP + DL" (31 MeV [67]), "foam" target (29 MeV [95]), foam with double layer "foam + DL" (60 MeV [96]), and "gratings" (2.3 MeV [69]). The color bar presents the laser contrast for each data point. The contrast values are given in the above references, typically for a few picoseconds or tens of picoseconds before the main pulse.

45 fs). The wavelength in all these cases is 800 nm. The trend of proton energies is as in the previous presented cases with two groups emerging depending on the laser intensity, as shown in **Figure 5A**. In the lower intensity group ($\lesssim 4 \times 10^{19}$ W cm^{-2}) the cut-off values are close, regardless of the target shape or type, with most of them in the few MeV range, excepting the 11 MeV peak of a submicron Al target that was obtained at a high contrast 10^{-10} [40]. Otherwise, at this level of intensities, nanostructuring the surface of the flat foils by adding micro- or nanospheres, or nanowires and nanoholes does not seem to bring any benefit. In the higher intensity range ($\gtrsim 5 \times 10^{19}$ W cm^{-2}) more peaks are observed, with the highest at 60 MeV delivered by a combination of double layer covered with foam [96]. Another peak at 29 MeV is obtained also for a foam target [95], although it is inferior to some Al targets which deliver both 40 MeV [36, 37]. It is worth mentioning that the contrast for all these 4 peaks is high, reaching the top value 10^{-11} for both foam targets. The double-layer targets perform almost similarly (10 to 20 MeV) at the micron size level or slightly below, and the contrast enhancement (from 10^{-6} to 10^{-10}) does not seem to improve their performance. In terms of pulse duration (**Figure 5B**), the foam targets with the highest energies have been operated at 30 fs compared to their Al counterparts at 45 fs. For most of the nanostructured targets the pulse duration was around 30–35 fs.

4 CONCLUSION

A survey of the main proton acceleration results published in the literature is presented, in support of the commissioning of experimental areas at ELI-NP, where solid targets will be irradiated with the 1 and 10 PW pulses. These results are organized according to the target morphology, i.e., geometry and constituents. The main laser parameters such as intensity, wavelength, pulse duration and for some cases the contrast are presented along. This is particularly useful for the sake of comparison, as the 1 and 10 PW pulses at ELI-NP are produced for pulse duration of ~ 25 fs. The current trend is towards the use of more sophisticated nano- and micro-structured targets which include different features on their surface such as nano-spheres, nano-rods, nano-holes, micropillars, foams, periodic trenches, etc. It appears that in these configurations the laser energy is converted into proton energy with a higher efficiency. An in-depth knowledge of the target characteristics is thus preferable in order to produce relevant experimental results which can be further compared with existing ones obtained by other groups or with numerical simulations. This study is rather intended as a general guide for target fabrication at ELI-NP which hosts a dedicated and fully equipped laboratory for this purpose. One general conclusion is that there are many opportunities for future experiments, considering the new direction in target fabrication and the advent of the 10 PW beams which are capable of producing intensities one order of magnitude higher than what has been so far utilized.

At ELI-NP, in the first phase (of the commissioning experiments at 1 PW) the laser power will be increased gradually while targets consisting of metallic foils (e.g., Al) will be utilized, with thickness in the few microns range. The goal is to assess the prepulse, the quality of the spot (diameter and the Strehl ratio) and the pointing stability. A plasma mirror is planned to be implemented shortly after in order to test submicron thick targets and to lower the back reflections that propagate to the laser bay. In the next phase, a series of experiments will utilize more advanced targets covered with nanowires and foams or consisting in double-layers, gratings and diamond-like carbon films. The choice is motivated by the high cut-off proton energies and also because of the relative readiness for providing these types of targets. In the multi-PW regime the QED effects such as radiation reaction and pair creation will have to be considered as they can affect the absorption of the laser energy and subsequently the electron heating and ion acceleration.

AUTHOR CONTRIBUTIONS

AM and CT conceived the paper with the contribution of all other authors.

FUNDING

We acknowledge funding from the project ELI-NP-Phase II (cofunded by the Romanian Government and the EU through the European Regional Development Fund), Programme Nucleu PN-19 06 01 05 (2021, 2022) together with LAPLAS VI contract No. 16N/2019 and IMPULSE (Grant Agreement #871161).

ACKNOWLEDGMENTS

The authors would like to thank J. Fuchs, S. N. Chen and K. Spohr for illuminating discussions.

REFERENCES

1. Snavely RA, Key MH, Hatchett SP, Cowan TE, Roth M, Phillips TW, et al. Intense High-Energy Proton Beams from Petawatt-Laser Irradiation of Solids. *Phys Rev Lett* (2000) 85:2945–8. doi:10.1103/PhysRevLett.85.2945
2. Higginson A, Gray RJ, King M, Dance RJ, Williamson SDR, Butler NMH, et al. Near-100 MeV Protons via a Laser-Driven Transparency-Enhanced Hybrid Acceleration Scheme. *Nat Commun* (2018) 9:724. doi:10.1038/s41467-018-03063-9
3. Frazer TP, Wilson R, King M, Butler NMH, Carroll DC, Duff MJ, et al. Enhanced Laser Intensity and Ion Acceleration Due to Self-Focusing in Relativistically Transparent Ultrathin Targets. *Phys Rev Res* (2020) 2: 042015. doi:10.1103/PhysRevResearch.2.042015
4. Roth M, Schollmeier M. Ion Acceleration—Target normal Sheath Acceleration. In: B Holzer, editor. Proceedings of the CAS-CERN Accelerator School: Plasma Wake Acceleration; 23–29 November 2014; Geneva, Switzerland. SPIE (2016).
5. Fuchs J, Antici P, d'Humières E, Lefebvre E, Borghesi M, Brambrink E, et al. Laser-driven Proton Scaling Laws and New Paths towards Energy Increase. *Nat Phys* (2006) 2:48–54. doi:10.1038/NPHYS199
6. Flippo KA, Workman J, Gautier DC, Letzring S, Johnson RP, Shimada T. Scaling Laws for Energetic Ions from the Commissioning of the New Los Alamos National Laboratory 200 TW Trident Laser. *Rev Sci Instr* (2008) 79: 10E534. doi:10.1063/1.2987678
7. Strickland D, Mourou G. Compression of Amplified Chirped Optical Pulses. *Opt Commun* (1985) 56:219–21. doi:10.1016/0030-4018(85)90120-8
8. Flippo KA, d'Humières E, Gaillard SA, Rassuchine J, Gautier DC, Schollmeier M, et al. Increased Efficiency of Short-Pulse Laser-Generated Proton Beams from Novel Flat-Top Cone Targets. *Phys Plasmas* (2008) 15:056709. doi:10.1063/1.2918125
9. Fukumi A, Nishiuchi M, Daido H, Li Z, Sagisaka A, Ogura K, et al. Laser Polarization Dependence of Proton Emission from a Thin Foil Target Irradiated by a 70fs, Intense Laser Pulse. *Phys Plasmas* (2005) 12:100701. doi:10.1063/1.2074988
10. Macchi A, Borghesi M, Passoni M. Ion Acceleration by Superintense Laser-Plasma Interaction. *Rev Mod Phys* (2013) 85:751–93. doi:10.1103/RevModPhys.85.751
11. Tanaka KA, Spohr KM, Balabanski DL, Balascuta S, Capponi L, Cernaianu MO, et al. Current Status and Highlights of the ELI-NP Research Program. *Matter Radiat Extremes* (2020) 5:024402. doi:10.1063/1.5093535
12. Doria D, Cernaianu MO, Ghenuche P, Stutman D, Tanaka KA, Ticos C, et al. Overview of ELI-NP Status and Laser Commissioning Experiments with 1 PW and 10 PW Class-Lasers. *J Inst* (2020) 15:C09053. doi:10.1088/1748-0221/15/09/C09053
13. Gheorghiu CC, Leca V, Popa D, Cernaianu MO, Stutman D. Overview on the Target Fabrication Facilities at ELI-NP and Ongoing Strategies. *J Inst* (2016) 11:C10011. doi:10.1088/1748-0221/11/10/c10011
14. Mora P. Plasma Expansion into a Vacuum. *Phys Rev Lett* (2003) 90:185002. doi:10.1103/PhysRevLett.90.185002

15. Zeil K, Kraft SD, Bock S, Bussmann M, Cowan TE, Kluge T, et al. The Scaling of Proton Energies in Ultrashort Pulse Laser Plasma Acceleration. *New J Phys* (2010) 12:045015. doi:10.1088/1367-2630/12/4/045015
16. Perego C, Batani D, Zani A, Passoni M. Target normal Sheath Acceleration Analytical Modeling, Comparative Study and Developments. *Rev Scientific Instr* (2012) 83:02B502. doi:10.1063/1.3666188
17. Passoni M, Perego C, Sgattoni A, Batani D. Advances in Target normal Sheath Acceleration Theory. *Phys Plasmas* (2013) 20:060701. doi:10.1063/1.4812708
18. Berger MJ, Coursey JS, Zucker MA, Chang J. *ESTAR, PSTAR, and ASTAR: Computer Programs for Calculating Stopping-Power and Range Tables for Electrons, Protons, and Helium Ions (Version 2.0.1).* Gaithersburg, MD: National Institute of Standards and Technology (2017). [Dataset]. doi:10.18434/T4NC7P
19. Bell AR, Davies JR, Guerin S, Ruhl H. Fast-electron Transport in High-Intensity Short-Pulse Laser - Solid Experiments. *Plasma Phys Control Fusion* (1997) 39:653–9. doi:10.1088/0741-3335/39/5/001
20. Li CK, Petrasso RD. Stopping of Directed Energetic Electrons in High-Temperature Hydrogenic Plasmas. *Phys Rev E* (2004) 70:067401. doi:10.1103/PhysRevE.70.067401
21. Chen CD, Li CK, Petrasso RD. *Comparison of Solid and Plasma Linear Energy Deposition for Electron Preheat and Fast Ignition Scenarios* (2006). [Dataset]. Available at: https://www.semanticscholar.org/paper/Comparison-of-solid-and-plasma-linear-energy-for-Chen Li/30696362f4858a3801462d7ce673c2f301cd2f34#citing-papers
22. Volpe L, Batani D, Morace A, Santos JJ. Collisional and Collective Effects in Two Dimensional Model for Fast-Electron Transport in Refluxing Regime. *Phys Plasmas* (2013) 20:013104. doi:10.1063/1.4771586
23. Wilks SC, Kruer WL, Tabak M, Langdon AB. Absorption of Ultra-Intense Laser Pulses. *Phys Rev Lett* (1992) 69:1383–6. doi:10.1103/physrevlett.69.1383
24. Hatchett SP, Brown CG, Cowan TE, Henry EA, Johnson JS, Key MH, et al. Electron, Photon, and Ion Beams from the Relativistic Interaction of Petawatt Laser Pulses with Solid Targets. *Phys Plasmas* (2000) 7:2076–82. doi:10.1063/1.874030
25. Flacco A, Ceccotti T, George H, Monot P, Martin P, Réau F, et al. Comparative Study of Laser Ion Acceleration with Different Contrast Enhancement Techniques. *Nucl Instr Methods Phys Res Section A: Acc Spectrometers, Detectors Assoc. Equip* (2010) 620:18–22. doi:10.1016/j.nima.2010.01.053
26. Batani D, Jafer R, Veltcheva M, Dezulian R, Lundh O, Lindau F, et al. Effects of Laser Prepulses on Laser-Induced Proton Generation. *New J Phys* (2010) 12:045018. doi:10.1088/1367-2630/12/4/045018
27. Kim I, Choi IW, Lee SK, Janulewicz KA, Sung JH, Yu TJ, et al. Spatio-temporal Characterization of Double Plasma Mirror for Ultrahigh Contrast and Stable Laser Pulse. *Appl Phys B* (2011) 104:81–6. doi:10.1007/s00340-011-4584-2
28. Lübcke A, Andreev AA, Höhm S, Grunwald R, Ehrentraut L, Schnürer M. Prospects of Target Nanostructuring for Laser Proton Acceleration. *Sci Rep* (2017) 7:44030. doi:10.1038/srep44030
29. Clark EL, Krushelnick K, Davies JR, Zepf M, Tatarakis M, Beg FN, et al. Measurements of Energetic Proton Transport through Magnetized Plasma from Intense Laser Interactions with Solids. *Phys Rev Lett* (2000) 84:670–3. doi:10.1103/PhysRevLett.84.670
30. Maksimchuk A, Gu S, Flippo K, Umstadter D, Bychenkov VY. Forward Ion Acceleration in Thin Films Driven by a High-Intensity Laser. *Phys Rev Lett* (2000) 84:4108–11. doi:10.1103/PhysRevLett.84.4108
31. Zepf M, Clark EL, Krushelnick K, Beg FN, Escoda C, Dangor AE, et al. Fast Particle Generation and Energy Transport in Laser-Solid Interactions. *Phys Plasmas* (2001) 8:2323–30. doi:10.1063/1.1351824
32. Flippo K, Maksimchuk A, Banerjee S, Wong V, Mourou G, Umstadter D, et al. Multi-mev Ion Beams from Terawatt Laser Thin-Foil Interactions. In: Proceedings of the IEEE Particle Accelerator Conference; 18–22 June 2001; Chicago, IL (2001). p. 2081–3. Conf.Proc.C 0106181. doi:10.1109/PAC.2001.987283
33. Hegelich M, Karsch S, Pretzler G, Habs D, Witte K, Guenther W, et al. MeV Ion Jets from Short-Pulse-Laser Interaction with Thin Foils. *Phys Rev Lett* (2002) 89:085002–08005. doi:10.1103/PhysRevLett.89.085002
34. McKenna P, Ledingham KWD, Shimizu S, Yang JM, Robson L, McCanny T, et al. Broad Energy Spectrum of Laser-Accelerated Protons for Spallation-Related Physics. *Phys Rev Lett* (2005) 94:084801–4. doi:10.1103/PhysRevLett.94.084801
35. McKenna P, Lindau F, Lundh O, Carroll DC, Clarke RJ, Ledingham KWD, et al. Low- and Medium-Mass Ion Acceleration Driven by Petawatt Laser Plasma Interactions. *Plasma Phys Control Fusion* (2007) 49:B223–B231. doi:10.1088/0741-3335/49/12b/s20
36. Ogura K, Nishiuchi M, Pirozhkov AS, Tanimoto T, Sagisaka A, Esirkepov TZ, et al. Proton Acceleration to 40 MeV Using a High Intensity, High Contrast Optical Parametric Chirped-Pulse amplification/Ti: Sapphire Hybrid Laser System. *Opt Lett* (2012) 37:2868–70. doi:10.1364/OL.37.002868
37. Green JS, Robinson APL, Booth N, Carroll DC, Dance RJ, Gray RJ, et al. High Efficiency Proton Beam Generation through Target Thickness Control in Femtosecond Laser-Plasma Interactions. *Appl Phys Lett* (2014) 104:214101. doi:10.1063/1.4879641
38. Palaniyappan S, Huang C, Gautier DC, Hamilton CE, Santiago MA, Kreuzer C, et al. Efficient Quasi-Monoenergetic Ion Beams from Laser-Driven Relativistic Plasmas. *Nat Commun* (2015) 6:10170. doi:10.1038/ncomms10170
39. Volpe L, Fedosejevs R, Gatti G, Pérez-Hernández JA, Méndez C, Apiñaniz J, et al. Generation of high energy laser-driven electron and proton sources with the 200 TW system VEGA 2 at the Centro de Laseres Pulsados. *High Pow Laser Sci Eng* (2019) 7:1–6. doi:10.1017/hpl.2019.10
40. Fourmaux S, Buffechoux S, Albertazzi B, Capelli D, Lévy A, Gnedyuk S, et al. Investigation of Laser-Driven Proton Acceleration Using Ultra-short, Ultra-intense Laser Pulses. *Phys Plasmas* (2013) 20:013110. doi:10.1063/1.4789748
41. Kaluza M, Schreiber J, Santala MIK, Tsakiris GD, Eidmann K, Meyer-ter-Vehn J, et al. Influence of the Laser Prepulse on Proton Acceleration in Thin-Foil Experiments. *Phys Rev Lett* (2004) 93:045003. doi:10.1103/PhysRevLett.93.045003
42. Lindau F, Lundh O, Persson A, McKenna P, Osvay K, Batani D, et al. Laser-accelerated Protons with Energy-dependent Beam Direction. *Phys Rev Lett* (2005) 95:175002. doi:10.1103/PhysRevLett.95.175002
43. Neely D, Foster P, Robinson A, Lindau F, Lundh O, Persson A, et al. Enhanced Proton Beams from Ultrathin Targets Driven by High Contrast Laser Pulses. *Appl Phys Lett* (2006) 89:021502. doi:10.1063/1.2220011
44. Flacco A, Sylla F, Veltcheva M, Carrié M, Nuter R, Lefebvre E, et al. Dependence on Pulse Duration and Foil Thickness in High-Contrast-Laser Proton Acceleration. *Phys Rev E* (2010) 81:036405. doi:10.1103/PhysRevE.81.036405
45. Fourmaux S, Buffechoux S, Gnedyuk S, Albertazzi B, Capelli D, Lecherbourg L, et al. Laser-based Proton Acceleration on Ultrathin Foil with a 100-TW-Class High Intensity Laser System. In: R Kashyap, M Têtu, RN Kleiman, editors. *Photonics North 2011*. . SPIE (2011). p. 156–62. doi:10.1117/12.905822
46. Roth M, Blazevic A, Geissel M, Schlegel T, Cowan TE, Allen M, et al. Energetic Ions Generated by Laser Pulses: a Detailed Study on Target Properties. *Phys Rev ST Accel Beams* (2002) 5:061301. doi:10.1103/PhysRevSTAB.5.061301
47. Fuchs J, Cowan TE, Audebert P, Ruhl H, Gremillet L, Kemp A, et al. Spatial Uniformity of Laser-Accelerated Ultrahigh-Current MeV Electron Propagation in Metals and Insulators. *Phys Rev Lett* (2003) 91:255002. doi:10.1103/PhysRevLett.91.255002
48. Kar S, Markey K, Simpson PT, Bellei C, Green JS, Nagel SR, et al. Dynamic Control of Laser-Produced Proton Beams. *Phys Rev Lett* (2008) 100:105004. doi:10.1103/PhysRevLett.100.105004
49. Busold S, Schumacher D, Brabetz C, Jahn D, Kroll F, Deppert O, et al. Towards Highest Peak Intensities for Ultra-short MeV-Range Ion Bunches. *Sci Rep* (2015) 5:12459. doi:10.1038/srep12459
50. Wagner F, Deppert O, Brabetz C, Fiala P, Kleinschmidt A, Poth P, et al. Maximum Proton Energy above 85 MeV from the Relativistic Interaction of Laser Pulses with Micrometer ThickCH2Targets. *Phys Rev Lett* (2016) 116:205002–6. doi:10.1103/PhysRevLett.116.205002
51. Khaghani D, Lobet M, Borm B, Burr L, Gärtner F, Gremillet L, et al. Enhancing Laser-Driven Proton Acceleration by Using Micro-pillar Arrays at High Drive Energy. *Sci Rep* (2017) 7:1–9. doi:10.1038/s41598-017-11589-z
52. Oishi Y, Nayuki T, Fujii T, Takizawa Y, Wang X, Yamazaki T, et al. Dependence on Laser Intensity and Pulse Duration in Proton Acceleration by Irradiation of Ultrashort Laser Pulses on a Cu Foil Target. *Phys Plasmas* (2005) 12:073102. doi:10.1063/1.1943436
53. Sinenian N, Fiksel G, Frenje JA, Freeman CG, Manuel MJ-E, Casey DT, et al. Heavy-ion Emission from Short-Pulse Laser-Plasma Interactions with Thin Foils. *Phys Plasmas* (2012) 19:093118. doi:10.1063/1.4754308

54. McKenna P, Ledingham KWD, Yang JM, Robson L, McCanny T, Shimizu S, et al. Characterization of Proton and Heavier Ion Acceleration in Ultrahigh-Intensity Laser Interactions with Heated Target Foils. *Phys Rev E* (2004) 70: 036405. doi:10.1103/PhysRevE.70.036405
55. Dover NP, Nishiuchi M, Sakaki H, Kondo K, Alkhimova MA, Faenov AY, et al. Effect of Small Focus on Electron Heating and Proton Acceleration in Ultrarelativistic Laser-Solid Interactions. *Phys Rev Lett* (2020) 124:084802. doi:10.1103/PhysRevLett.124.084802
56. Kar S, Markey K, Borghesi M, Carroll DC, McKenna P, Neely D, et al. Ballistic Focusing of Polyenergetic Protons Driven by Petawatt Laser Pulses. *Phys Rev Lett* (2011) 106:225003–6. doi:10.1103/PhysRevLett.106.225003
57. Schnürer M, Andreev AA, Steinke S, Sokollik T, Paasch-Colberg T, Nickles PV, et al. Comparison of Femtosecond Laser-Driven Proton Acceleration Using Nanometer and Micrometer Thick Target Foils. *Laser Part Beams* (2011) 29: 437–46. doi:10.1017/S0263034611000553
58. Steinke S, Bin JH, Park J, Ji Q, Nakamura K, Gonsalves AJ, et al. Acceleration of High Charge Ion Beams with Achromatic Divergence by Petawatt Laser Pulses. *Phys Rev Accel Beams* (2020) 23:021302. doi:10.1103/PhysRevAccelBeams.23.021302
59. Gizzi LA, Cristoforetti G, Baffigi F, Brandi F, D'Arrigo G, Fazzi A, et al. Intense Proton Acceleration in Ultrarelativistic Interaction with Nanochannels. *Phys Rev Res* (2020) 2:033451–6. doi:10.1103/PhysRevResearch.2.033451
60. Murakami Y, Kitagawa Y, Sentoku Y, Mori M, Kodama R, Tanaka KA, et al. Observation of Proton Rear Emission and Possible Gigagauss Scale Magnetic fields from Ultra-intense Laser Illuminated Plastic Target. *Phys Plasmas* (2001) 8:4138–43. doi:10.1063/1.1390333
61. Hornung J, Zobus Y, Boller P, Brabetz C, Eisenbarth U, Kühl T, et al. Enhancement of the Laser-Driven Proton Source at PHELIX. *High Pow Laser Sci Eng* (2020) 8:1–8. doi:10.1017/hpl.2020.23
62. Okihara S, Sentoku Y, Sueda K, Shimizu S, Sato F, Miyanaga N, et al. Energetic Proton Generation in a Thin Plastic Foil Irradiated by Intense Femtosecond Lasers. *J Nucl Sci Technol* (2002) 39:1–5. doi:10.1080/18811248.2002.9715150
63. Ter-Avetisyan S, Nickles PV. Ion Acceleration at the Front and Rear Surfaces of Thin Foils with High-Intensity 40-fs Laser Pulses. *Jetp Lett* (2006) 83: 206–10. doi:10.1134/S0021364006050055
64. Ceccotti T, Lévy A, Popescu H, Réau F, D'Oliveira P, Monot P, et al. Proton Acceleration with High-Intensity Ultrahigh-Contrast Laser Pulses. *Phys Rev Lett* (2007) 99:185002. doi:10.1103/PhysRevLett.99.185002
65. Dollar F, Zulick C, Thomas AGR, Chvykov V, Davis J, Kalinchenko G, et al. Finite Spot Effects on Radiation Pressure Acceleration from Intense High-Contrast Laser Interactions with Thin Targets. *Phys Rev Lett* (2012) 108: 175005–10. doi:10.1103/PhysRevLett.108.175005
66. Floquet V, Klimo O, Psikal J, Velyhan A, Limpouch J, Proska J, et al. Microsphere Layered Targets Efficiency in Laser Driven Proton Acceleration. *J Appl Phys* (2013) 114:083305. doi:10.1063/1.4819239
67. Margarone D, Kim IJ, Psikal J, Kaufman J, Mocek T, Choi IW, et al. Laser-driven High-Energy Proton Beam with Homogeneous Spatial Profile from a Nanosphere Target. *Phys Rev ST Accel Beams* (2015) 18:071304–11. doi:10.1103/PhysRevSTAB.18.071304
68. Yogo A, Daido H, Bulanov SV, Nemoto K, Oishi Y, Nayuki T, et al. Laser Ion Acceleration via Control of the Near-Critical Density Target. *Phys Rev E* (2008) 77:016401. doi:10.1103/PhysRevE.77.016401
69. Giuffrida L, Svensson K, Psikal J, Margarone D, Lutoslawski P, Scuderi V, et al. Nano and Micro Structured Targets to Modulate the Spatial Profile of Laser Driven Proton Beams. *J Inst* (2017) 12:C03040. doi:10.1088/1748-0221/12/03/c03040
70. McIlvenny A, Ahmed H, Scullion C, Doria D, Romagnani L, Martin P, et al. Characteristics of Ion Beams Generated in the Interaction of Ultra-short Laser Pulses with Ultra-thin Foils. *Plasma Phys Control Fusion* (2020) 62:054001. doi:10.1088/1361-6587/ab7d26
71. Poole PL, Obst L, Cochran GE, Metzkes J, Schlenvoigt H-P, Prencipe I, et al. Laser-driven Ion Acceleration via Target normal Sheath Acceleration in the Relativistic Transparency Regime. *New J Phys* (2018) 20:013019. doi:10.1088/1367-2630/aa9d47
72. Ebert T, Neumann NW, Döhl LNK, Jarrett J, Baird C, Heathcote R, et al. Enhanced Brightness of a Laser-Driven X-ray and Particle Source by Microstructured Surfaces of Silicon Targets. *Phys Plasmas* (2020) 27: 043106. doi:10.1063/1.5125775
73. Geng YX, Wu D, Yu W, Sheng ZM, Fritzsche S, Liao Q, et al. Proton Beams from Intense Laser-Solid Interaction: Effects of the Target Materials. *Matter Radiat Extremes* (2020) 5:064402. doi:10.1063/5.0014854
74. Gaillard SA, Kluge T, Flippo KA, Bussmann M, Gall B, Lockard T, et al. Increased Laser-Accelerated Proton Energies via Direct Laser-Light-Pressure Acceleration of Electrons in Microcone Targets. *Phys Plasmas* (2011) 18: 056710. doi:10.1063/1.3575624
75. Antici P, Gaillard S, Gremillet L, Amin M, Nakatsutsumi M, Romagnani L, et al. Optimization of Flat-Cone Targets for Enhanced Laser-Acceleration of Protons. *Nucl Instr Methods Phys Res Section A: Acc Spectrometers, Detectors Assoc Equip* (2010) 620:14–7. doi:10.1016/j.nima.2010.01.052
76. Foord ME, Bartal T, Bellei C, Key M, Flippo K, Stephens RB, et al. Proton Trajectories and Electric fields in a Laser-Accelerated Focused Proton Beam. *Phys Plasmas* (2012) 19:056702. doi:10.1063/1.3700181
77. Sentoku Y, Mima K, Ruhl H, Toyama Y, Kodama R, Cowan TE. Laser Light and Hot Electron Micro Focusing Using a Conical Target. *Phys Plasmas* (2004) 11:3083–7. doi:10.1063/1.1735734
78. Budriga O, Ionel LE, Tatomirescu D, Tanaka KA. Enhancement of Laser-Focused Intensity Greater Than 10 Times through a Re-entrant Cone in the Petawatt Regime. *Opt Lett* (2020) 45:3454–7. doi:10.1364/OL.395316
79. Buffechoux S, Psikal J, Nakatsutsumi M, Romagnani L, Andreev A, Zeil K, et al. Hot Electrons Transverse Refluxing in Ultraintense Laser-Solid Interactions. *Phys Rev Lett* (2010) 105:015005. doi:10.1103/PhysRevLett.105.015005
80. Sokollik T, Schnürer M, Steinke S, Nickles PV, Sandner W, Amin M, et al. Directional Laser-Driven Ion Acceleration from Microspheres. *Phys Rev Lett* (2009) 103:135003–7. doi:10.1103/PhysRevLett.103.135003
81. Sokollik T, Paasch-Colberg T, Gorling K, Eichmann U, Schnürer M, Steinke S, et al. Laser-driven Ion Acceleration Using Isolated Mass-Limited Spheres. *New J Phys* (2010) 12:113013. doi:10.1088/1367-2630/12/11/113013
82. Hilz P, Ostermayr TM, Huebl A, Bagnoud V, Borm B, Bussmann M, et al. Isolated Proton bunch Acceleration by a Petawatt Laser Pulse. *Nat Commun* (2018) 9:423. doi:10.1038/s41467-017-02663-1
83. Schnurer M, Ter-avetisyan S, Busch S, Risse E, Kalachnikov MP, Sandner W, et al. Ion Acceleration with Ultrafast Laser Driven Water Droplets. *Laser Part Beams* (2005) 23:337–43. doi:10.1017/s0263034605050482
84. Becker GA, Schwab MB, Lötzsch R, Tietze S, Klöpfel D, Rehwald M, et al. Characterization of Laser-Driven Proton Acceleration from Water Microdroplets. *Sci Rep* (2019) 9:17169. doi:10.1038/s41598-019-53587-3
85. Burza M, Gonoskov A, Genoud G, Persson A, Svensson K, Quinn M, et al. Hollow Microspheres as Targets for Staged Laser-Driven Proton Acceleration. *New J Phys* (2011) 13:013030. doi:10.1088/1367-2630/13/1/013030
86. Henig A, Kiefer D, Geissler M, Rykovanov SG, Ramis R, Hörlein R, et al. Laser-driven Shock Acceleration of Ion Beams from Spherical Mass-Limited Targets. *Phys Rev Lett* (2009) 102:095002. doi:10.1103/PhysRevLett.102.095002
87. Ostermayr TM, Haffa D, Hilz P, Pauw V, Allinger K, Bamberg K-U, et al. Proton Acceleration by Irradiation of Isolated Spheres with an Intense Laser Pulse. *Phys Rev E* (2016) 94:033208. doi:10.1103/PhysRevE.94.033208
88. Vallières S, Salvadori M, Permogorov A, Cantono G, Svendsen K, Chen Z, et al. Enhanced Laser-Driven Proton Acceleration Using Nanowire Targets. *Sci Rep* (2021) 11:2226. doi:10.1038/s41598-020-80392-0
89. Bailly-Grandvaux M, Kawahito D, McGuffey C, Strehlow J, Edghill B, Wei MS, et al. Ion Acceleration from Microstructured Targets Irradiated by High-Intensity Picosecond Laser Pulses. *Phys Rev E* (2020) 102:021201. doi:10.1103/PhysRevE.102.021201
90. Cantono G, Permogorov A, Ferri J, Smetanina E, Dmitriev A, Persson A, et al. Laser-driven Proton Acceleration from Ultrathin Foils with Nanoholes. *Sci Rep* (2021) 11:5006. doi:10.1038/s41598-021-84264-z
91. Vallières S, Barberio M, Scisciò M, d'Humières E, Antici P. Enhanced Laser-Driven Proton Acceleration Using Ultrasmall Nanoparticles. *Phys Rev Accel Beams* (2019) 22:091303–1/6. doi:10.1103/PhysRevAccelBeams.22.091303
92. Margarone D, Klimo O, Kim IJ, Prokůpek J, Limpouch J, Jeong TM, et al. Laser-driven Proton Acceleration Enhancement by Nanostructured Foils. *Phys Rev Lett* (2012) 109:234801–1/5. doi:10.1103/PhysRevLett.109.234801
93. Schwoerer H, Pfotenhauer S, Jäckel O, Amthor K-U, Liesfeld B, Ziegler W, et al. Laser-plasma Acceleration of Quasi-Monoenergetic Protons from Microstructured Targets. *Nature* (2006) 439:445–8. doi:10.1038/nature04492

94. Fedeli L, Formenti A, Cialfi L, Pazzaglia A, Passoni M. Ultra-intense Laser Interaction with Nanostructured Near-Critical Plasmas. *Sci Rep* (2018) 8:3834. doi:10.1038/s41598-018-22147-6
95. Prencipe I, Sgattoni A, Dellasega D, Fedeli L, Cialfi L, Choi IW, et al. Development of Foam-Based Layered Targets for Laser-Driven Ion Beam Production. *Plasma Phys Control Fusion* (2016) 58:034019. doi:10.1088/0741-3335/58/3/034019
96. Ma WJ, Kim IJ, Yu JQ, Choi IW, Singh PK, Lee HW, et al. Laser Acceleration of Highly Energetic Carbon Ions Using a Double-Layer Target Composed of Slightly Underdense Plasma and Ultrathin Foil. *Phys Rev Lett* (2019) 122: 014803–1/4. doi:10.1103/PhysRevLett.122.014803
97. Schollmeier M, Becker S, Geißel M, Flippo KA, Blažević A, Gaillard SA, et al. Controlled Transport and Focusing of Laser-Accelerated Protons with Miniature Magnetic Devices. *Phys Rev Lett* (2008) 101:055004–1/4. doi:10.1103/PhysRevLett.101.055004
98. Ceccotti T, Floquet V, Sgattoni A, Bigongiari A, Klimo O, Raynaud M, et al. Evidence of Resonant Surface-Wave Excitation in the Relativistic Regime through Measurements of Proton Acceleration from Grating Targets. *Phys Rev Lett* (2013) 111:185001–1/5. doi:10.1103/PhysRevLett.111.185001

Conflict of Interest: The authors declare that the research was conducted in the absence of any commercial or financial relationships that could be construed as a potential conflict of interest.